Water Resources Research

RESEARCH ARTICLE
10.1029/2023WR034692

A Simple Model of Flood Peak Attenuation

Rodrigo C. D. Paiva[1] and **Stefany G. Lima**[1]

[1]Institute of Hydraulic Research, Federal University of Rio Grande do Sul (UFRGS), Porto Alegre, Brazil

Special Section:
Advancing flood characterization, modeling, and communication

Rodrigo Cauduro Dias de Paiva and Stefany Goncalves Lima contributed equally to this work.

Key Points:

- A simple physically-based analytical model of flood wave peak attenuation is developed
- The model is validated using numerical solutions of the Saint-Venant equations and observations of historical dam breaks and natural floods
- Flood wave attenuation is governed mostly by initial peak discharge, volume, floodplain storage, and river slope

Supporting Information:

Supporting Information may be found in the online version of this article.

Correspondence to:

R. C. D. Paiva and S. G. Lima,
rodrigo.paiva@ufrgs.br;
stefglima@gmail.com

Citation:

Paiva, R. C. D., & Lima, S. G. (2024). A simple model of flood peak attenuation. *Water Resources Research*, *60*, e2023WR034692. https://doi.org/10.1029/2023WR034692

Received 17 FEB 2023
Accepted 23 NOV 2023

Author Contributions:

Conceptualization: Rodrigo C. D. Paiva, Stefany G. Lima
Data curation: Rodrigo C. D. Paiva, Stefany G. Lima

Abstract A simple analytical model was developed for evaluating the attenuation of flood wave peak discharge. The physically-based model represents the flood wave along its trajectory, based on the diffusive model. Relative peak discharge decreases along the downstream distance according to a power function. The distance is scaled by the attenuation factor related to river hydrodynamics (flow rating, hydraulic diffusivity, celerity, and floodplain storage) and input hydrograph (initial peak discharge, hydrograph volume, and its relative curvature). It also informs the attenuation length, which is a practical indicator of the river distance in which discharge decreases by a given factor. Sensitivity analyses indicate that initial peak discharge, volume, floodplain storage, and slope are the governing factors of attenuation. Model's validity and accuracy were demonstrated by reproducing data from (a) numerical solutions of the Saint-Venant equations covering a wide range of conditions, (b) 29 observations from 11 historical dam-breaks, (c) 15 observations of natural floods in seven rivers and (d) a detailed hydrodynamic model. The model errors were generally lower than 10% and not larger than the typical uncertainty of flood observations. The accuracy is higher than simplified empirical models and analogous to a detailed hydrodynamic model that is representative of current practice. The proposed flood attenuation model can be easily applied using a few common parameters and a simple equation in a basic spreadsheet. It is suitable for practical applications such as first assessments of natural and dam-break floods, engineering design, and analyses of large river networks supported by remote sensing data.

Plain Language Summary Floods are the most common and damaging natural disaster. Predicting how flood waves weaken while traveling along rivers is key to clarifying the risks of natural and dam-break floods, in engineering design, reservoir operation, and environmental analysis. We developed a simple and innovative physical model of flood wave attenuation. This model was accurate when tested against observations from historical dam-break and natural floods and sophisticated computer simulations covering a wide range of river types and flow conditions. Flood waves weaken more when their peak is large, their volume is low, and in low-slope rivers with large floodplains. This simple and meaningful equation can be easily applied for practical applications and help with massive mapping of floods over large regions.

1. Introduction

Floods are the most common and damaging natural hazard (Blöschl, 2022; Mishra et al., 2022). Disastrous river floods are caused by either natural processes, such as heavy rainfall, or the failure of hydraulic structures such as dams (ICOLD, 2022; Merz et al., 2021). Furthermore, floods are the major driving force of river-floodplain ecological processes (Junk et al., 1989; Poff et al., 1997). As flood waves propagate downstream, they rise river discharge, water depths and velocities. A fundamental question is how they evolve in terms of their propagation speed, shape, volume, especially their peak magnitude (Chow et al., 1988; Dingman, 2009; Ponce, 2014). Although floods may change because of land use and climate change, river-floodplain processes and hydraulic interventions can significantly affect flood waves (Blöschl, 2022; Brunner et al., 2021; Fleischmann et al., 2016; Merz et al., 2021; Paiva et al., 2013; T. H. Wong & Laurenson, 1983). Understanding these processes and how flood waves weaken while traveling along rivers is key for estimating and managing risks associated with both natural and dam-break floods, but also for engineering design, reservoir operation, and environmental analyses.

Flood waves have been widely investigated for decades (Yevjevich, 1964). Documentations range from Saint Venant's early work defining the fundamental laws of mass and momentum conservation (Saint-Venant, 1871) to the observation and definition of flood propagation celerity (Seddon, 1900), its diffusion and attenuation (Hayami, 1951), and its dominant kinematic nature (Lighthill & Whitham, 1955).

Given the inherent complexity of this natural phenomenon and equations, the field evolved with a significant focus on computer-aided numerical methods for solving the fundamental flow laws. Flood waves can be simulated

Formal analysis: Rodrigo C. D. Paiva, Stefany G. Lima
Funding acquisition: Rodrigo C. D. Paiva
Investigation: Rodrigo C. D. Paiva, Stefany G. Lima
Methodology: Rodrigo C. D. Paiva
Project Administration: Rodrigo C. D. Paiva
Resources: Rodrigo C. D. Paiva
Software: Rodrigo C. D. Paiva, Stefany G. Lima
Supervision: Rodrigo C. D. Paiva
Validation: Rodrigo C. D. Paiva, Stefany G. Lima
Visualization: Rodrigo C. D. Paiva, Stefany G. Lima
Writing – original draft: Rodrigo C. D. Paiva
Writing – review & editing: Rodrigo C. D. Paiva, Stefany G. Lima

using simplified and limited flow routing Muskingum and Muskingum-Cunge-Dooge methods (Cunge, 1969; Dooge, 1973; Koussis, 2009; McCarthy, 1938), which are commonly introduced in hydrology textbooks (e.g., Chow et al., 1988; Dingman, 2009; Ponce, 2014) and used in distributed hydrological models (e.g., Arnold et al., 1998; David et al., 2016; Thober et al., 2019). A great effort has been placed on computational hydraulics since the 50s (Cunge & Hager, 2015) and current hydrodynamic models (Teng et al., 2017) can solve full Saint-Venant or 2D shallow water equations providing a detailed representation of floods at local (USACE, 2020), regional/continental (Buttinger-Kreuzhuber et al., 2022; Hodges, 2013; Paiva et al., 2013; Siqueira et al., 2018), and global scales (Sampson et al., 2015; Wood et al., 2011; Yamazaki et al., 2011) including complex terrain, land use and hydraulic infrastructure complexities. For instance, a popular representative of current flood modeling practice is HEC-RAS software (USACE, 2020). Typical applications usually involve defining geometry from terrain/bathymetry maps, boundary conditions, solving flow equations using sophisticated finite differences/volume numerical methods and interpreting results. These methods require expert knowledge for controlling numerical errors and uncertainties, in addition to input data, preparation time and computational costs that may limit their large-scale application over multiple scenarios.

Alternatively, direct analytical solutions of physical models could provide a deeper understanding of the governing factors in flood wave attenuation and simple first-order approximations for engineering practice and comprehension of natural river-floodplain systems. It could also enable robust analysis of extensive national-global river networks (e.g., ANA, 2017; Lehner & Grill, 2013; Moore et al., 2019), especially when enhanced by information from remote sensing technology, such as the recently launched SWOT satellite (Biancamaria et al., 2016).

Past studies have proposed analytical, semi-analytical, and empirical solutions of the fundamental laws describing flood waves, but they are limited in representing flood peak attenuation. For instance, analytical profiles of the (a) dam-break flood wave under simplified assumptions (Chanson, 2004) and the (b) monoclinal rising wave (Henderson, 1966) do not represent flood peak attenuation. (c) Exponential amplitude attenuation of sinusoidal waves using harmonic or small perturbation linear analyses (Fenton, 2019; Kundzewicz & Dooge, 1989; Ponce & Simons, 1977; Ponce et al., 2003; V. P. Singh et al., 1998; Tsai & Yen, 2001) are conceptually inaccurate for attenuation of floodwaves. (d) Unit hydrograph solutions of dynamic and diffusive wave approximation coupled with numerical convolution (Brutsaert, 2005; Dooge, 1973; Hayami, 1951) are as costly and limited as simplified Muskingum methods. Empirical models of flood peak attenuation built from (e) numerical simulations (e.g., Rossi et al., 2021; Rutschmann & Hager, 1996; Wetmore & Fread, 1981) or from (f) dam-break observations (e.g., Costa, 1985; United States Bureau of Reclamation - USBR, 1989) are either oversimplified by not accounting for all governing factors (e.g., only river distance) or impractical when developed as only a few abacus for some flow conditions.

Despite these past efforts, no general model has been developed that can be easily applied using a simple and meaningful equation and a few commonly available parameters to accurately answer the fundamental question: how does the flood wave peak attenuate?

This paper presents a simple physically based analytical model of flood wave discharge peak attenuation. We discuss the model development along with interpretations (Section 2) and explore the governing factors of attenuation by employing analytical reasoning (Section 2) and sensitivity analyses (Section 3). The model validity and accuracy are evaluated with validations against numerical simulations for a wide range of river characteristics and flow conditions (Section 3), multiple observations from historical dam breaks (Section 4) and natural floods (Section 5), and a detailed hydrodynamic model (Section 6). Model performance is compared to a simplified empirical model (Section 4) and a hydrodynamic model representative of current practice (Section 6). The feasibility of the model for practical applications is also discussed.

2. The Flood Attenuation Model

The flood attenuation model (Figure 1) is developed to predict the attenuation of flood wave peak discharge. The model is based on (a) physical principles and can be (b) easily applied using a simple equation and (c) a few commonly available parameters related to river characteristics and inflow hydrographs. It represents (d) the flood wave along its travel path (Figure 1c), based on the diffusive wave with inertial effects. The model (e) assumes that the hydrograph and wave profile have constant shape and volume (Figures 1b and 1c), and it accounts for (f) a generic discharge rating, (g) floodplain storage, (h) looped rating curve effects, and (i) variable celerity and hydraulic diffusivity.

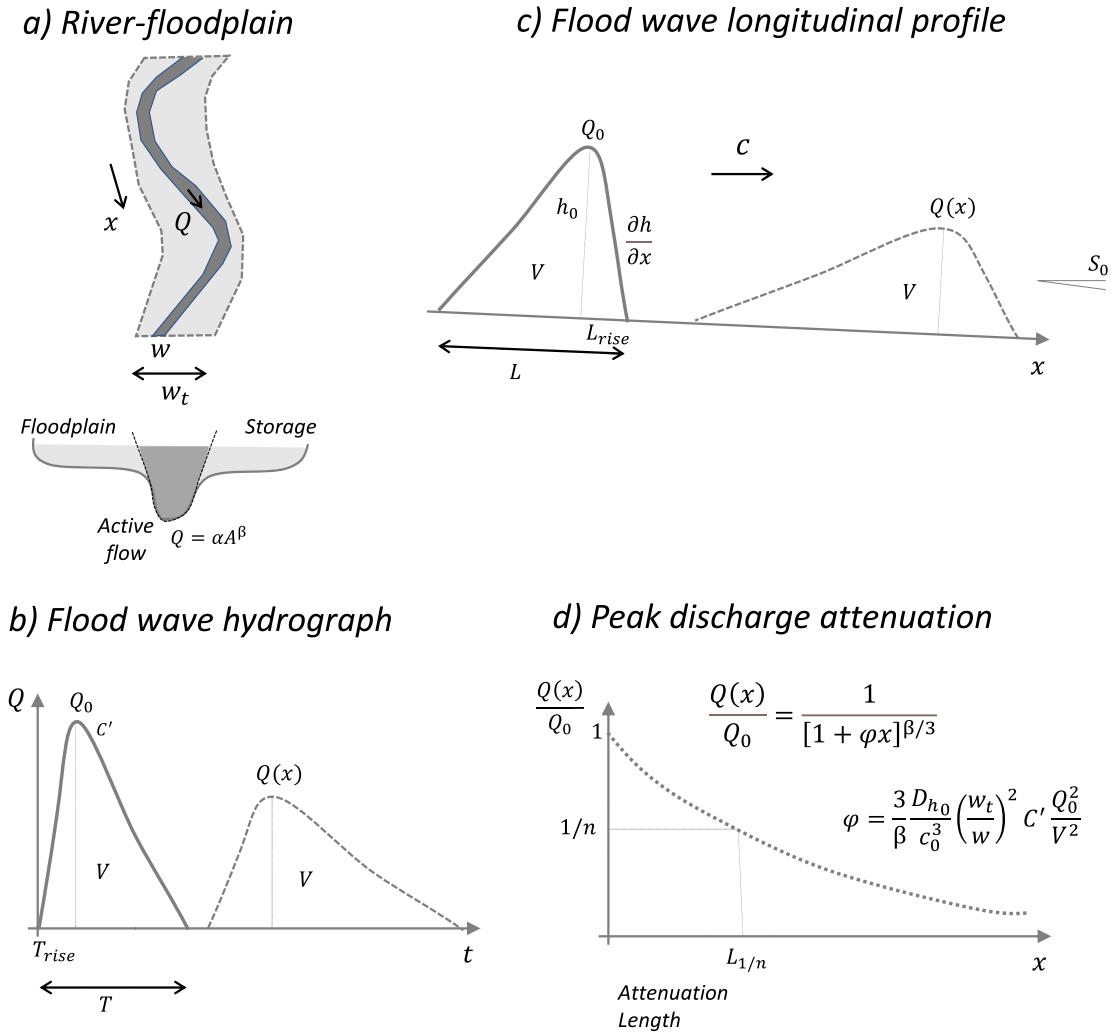

Figure 1. Representation of the flood wave by the flood attenuation model: (a) Active flow river cross-section with wetted area A and flow rating parameters α and β and floodplain storage as the ratio between floodplain and river width $\left(\frac{w_t}{w}\right)$; (b) Discharge hydrographs with constant volume V, shape, and relative curvature C' at the peak; (c) Discharge longitudinal profile showing the flood wave traveling downstream with celerity c and hydraulic diffusivity D_h; (d) The flood attenuation model predicting peak discharge Q_p reduction along main river distance x from Q_0 to $Q(x)$ as a function of the attenuation factor φ.

The model summary and main equation are shown in Figure 1d. The next sections describe the model in detail.

2.1. The Diffusion Wave Model

The Saint-Venant equations represent 1D unsteady and gradually varied free surface flows, by accounting for mass and momentum conservation and balancing inertia, gravitational, pressure and friction forces, for long waves with constant water density, and very small stream line curvature and vertical acceleration (Dingman, 2009; Ponce, 2014; Saint-Venant, 1871). The diffusion wave model is a simplification of the Saint-Venant equations assuming that acceleration and inertial terms are negligible. It has been found to be applicable for most river flood waves (e.g., Getirana & Paiva, 2013) and it is described in several publications (e.g., Dingman, 2009; Hayami, 1951; Lighthill & Whitham, 1955; Ponce, 2014). It predicts the propagation of the flood wave discharge Q along the river channel distance x over time t:

$$\frac{\partial Q}{\partial t} + c\frac{\partial Q}{\partial x} = D_h\frac{\partial^2 Q}{\partial x^2} \quad (1)$$

This model accounts for the translation of the flood wave along the river channel with a velocity called the kinematic wave celerity c and its diffusion as a function of the spatial curvature of discharge $\frac{\partial^2 Q}{\partial x^2}$ and hydraulic diffusivity D_h.

The kinematic wave celerity c (Lighthill & Whitham, 1955; Seddon, 1900) is defined by the ratio of changing discharge versus storage represented by the cross-sectional area A (here including active flow and storage areas):

$$c = \frac{\partial Q}{\partial A} \tag{2}$$

The hydraulic diffusivity, caused by gravitational, friction, and pressure forces, and including inertial effects (Dooge, 1973; Hayami, 1951; Ponce, 1991b) is defined as:

$$D_h = \frac{Q}{2wS}\left(1 - \upsilon^2\right) \tag{3}$$

where w is the top flow width, and S is the frictional slope, which is assumed as the water surface slope. The Vedernikov number $\upsilon = (c - U)/c_d$ is the ratio between the relative kinematic $c - U$ and dynamic wave celerity $c_d = (gh)^{0.5}$, in which h is the hydraulic depth and $U = Q/A$ is the flow velocity (Ponce, 1991b).

The next sections discuss how to estimate or parametrize each of the diffusion model variables and how to solve it to estimate flood peak discharge along the distance x.

2.2. Flood Wave Celerity

Discharge is usually expressed as a function of active flow area (Figure 1a):

$$Q = \alpha A^{\beta} \tag{4}$$

and it is well known (Chow, 1959; Dingman, 2009; Ponce, 2014; Seddon, 1900) that the flood wave celerity can be estimated (after applying Equation 2) as a function of the flow velocity:

$$c = \beta U$$

or expressed as a function of discharge:

$$c = \alpha^{\frac{1}{\beta}} \beta Q^{1-\frac{1}{\beta}} \tag{5}$$

The rating exponent β represents the rate at which discharge increases with rising water. There is a vast literature concerning how α and β can vary considering different water flow regimes (e.g., laminar or turbulent), resistance models (e.g., Chezy or Manning–Strickler), cross-section geometry, bed roughness, and even for mud and debris flows. The most typical approximation for natural rivers is turbulent water flow using the Manning–Strickler equation over a wide rectangular channel, where $Q = \frac{1}{n} w h^{\frac{5}{3}} S^{0.5}$, $\beta = 5/3$, $\alpha = \frac{S^{0.5}}{n W^{\frac{2}{3}}}$ (T. S. Wong & Zhou, 2006), and the celerity and depth are computed as:

$$c = \frac{5}{3}\frac{Q^{0.4} S^{0.3}}{n^{0.6} w^{0.4}}, \quad h = \left(\frac{Qn}{wS^{0.5}}\right)^{\frac{3}{5}} \tag{6}$$

For laminar flows, $\beta = 3$ (Ponce, 2014), and for mud and debris flows, $\beta \sim 1.5$–3 (Julien & Paris, 2010; Prochaska et al., 2008). Additionally, β can increase by more than 0.16 depending on the roughness variation with depth (Jarrett, 1984), reaching values larger than $\beta = 1.86$ (Collischonn et al., 2017), even for natural rivers.

2.3. Floodplain Storage

Flood waves on rivers with extensive floodplains present decreased celerity, as observed by T. H. Wong and Laurenson (1983). Floodplains usually present low velocities, acting as storage areas that delay flood wave hydrographs (e.g., Paiva et al., 2013). Whereas celerity in natural rivers is observed from 1 to a few m/s for in

bank flows, it can decrease to less than 0.2 m/s due to floodplains effects (Meyer et al., 2018; T. H. Wong & Laurenson, 1983). Consequently, the celerity relations for main channel active flow (Section 2.2) are usually not valid above river bankfull conditions.

The floodplain storage parameter is defined here as the ratio of w_t /w, where the active channel top flow width is w and the total river-floodplain width is w_t (Figure 1a). Meandering rivers with larger main channel lengths, compared with the floodplain flow path length, can also be accounted for by estimating w_t as the total flooded area divided by the main river length, or by correcting it using the ratio of valley and river lengths. In addition, the floodplain storage parameter can be either constant or modeled as increasing with discharge.

From Equation 2, the celerity can be simply corrected by reducing the main channel's celerity (Equation 5) as a function of the floodplain size (see also Dingman, 2009):

$$\frac{c}{(w_t/w)} \tag{7}$$

Similarly, from Equation 3, the main channel hydraulic diffusivity can be easily adjusted:

$$\frac{D_h}{(w_t/w)} \tag{8}$$

Thus, the floodplain storage reduces both flood kinematic wave celerity and hydraulic diffusivity by the relative size of the total river-floodplain storage width compared with the active flow width. This correction is valid for cases where floodplains act primarily as storage areas. Active floodplains with significant flow velocities (e.g., flash floods over canyon valleys) should be accounted in the active flow area and respective flow rating (Equation 4) and celerity (Equation 5) estimates.

2.4. Looped Rating Curve Effects on Celerity

Flood wave celerity is usually estimated considering a single discharge rating relation (e.g., Equations 4–6). However, dynamic flood waves with large and/or rapid variations of water depth in low-slope rivers can present looped rating curves (e.g., Meade et al., 1991). In the first case, the water surface slope can usually be approximated by the terrain slope S_0, but in the latter, it can be impacted by variations in water depth and approximated by $S_0 + \frac{\partial h}{\partial x}$ (Figure 1c). Discharge from a looped rating can be corrected using the Jones formula (Henderson, 1966), and a similar argument is extended herein for celerity. In this case, when flow velocity and c is estimated based on $S_0^{0.5}$, it can be corrected by:

$$c^* = c\left(1 + \frac{\frac{\partial h}{\partial x}}{S_0}\right)^{0.5} \tag{9}$$

If the water depth gradient in a flood wavefront is approximated as a function of the maximum water depth h_0 and its length estimated as $L_{rise} = c^* T_{rise}$, then the celerity is corrected with a few iterations, expressed as:

$$c^* = c\left(1 + \frac{h_0}{c^* T_{rise} S_0}\right)^{0.5} \tag{10}$$

For instance, rapidly varying flood waves moving over low-slope rivers (<1 m/km) can cause considerable increases in surface water slopes and celerity.

2.5. Flood Wave and Hydrograph Curvature

The flood wave usually propagates downstream while it attenuates its discharge peak and increases its base time and length, conserving total volume. The degree of such attenuation is a function of the curvature of the discharge profile and hydrograph, as $\frac{\partial^2 Q}{\partial x^2} = \frac{1}{c^2}\frac{\partial^2 Q}{\partial t^2}$ when advection effects prevail over diffusion (from Equation 1). In this section, we seek to understand such curvature in other estimate flood peak attenuation from the diffusion model (Equation 1). Although Lighthill and Whitham (1955) suggest that this curvature can be informed by observations, it can be either impractical or inaccurate because it is not constant. The flood wave hydrograph and profile

are approximated here using a predefined shape, as illustrated in Figures 1b and 1c. A reasonable first approximation is a triangular shape, where the discharge peak Q_p, the base of the hydrograph (wave period) T, and the total volume V are interrelated by:

$$V = \frac{Q_p T}{2} \tag{11}$$

The hydrograph rising and falling limb times can be defined as $\frac{sT}{2}$ and $\frac{(2-s)T}{2}$, where the asymmetry parameter $s = 1$ indicates a symmetric hydrograph, and $0 < s < 1$ represents faster rising limbs.

Assuming a triangular shape (Figures 1b and 1c), the temporal curvature at the discharge peak can be approximated over a time length δT:

$$\frac{\partial^2 Q}{\partial t^2} = \frac{\partial}{\partial t}\left(\frac{\partial Q}{\partial t}\right) \approx \left(\frac{-Q_p}{T_{rise}} - \frac{Q_p}{T_{fall}}\right)/\delta T \tag{12}$$

and the above relations can be expressed as a function of hydrograph peak and volume:

$$\frac{\partial^2 Q}{\partial t^2} = -C' \frac{{Q_p}^3}{V^2} \tag{13}$$

where $C' \approx \frac{1}{s(2-s)\delta}$ is defined as the relative curvature at the discharge peak, which is only a function of the predefined shape. From this definition, an asymmetric hydrograph has larger relative curvature. Furthermore, the exponents of Equation 13 denote the major role of peak discharge, increasing the absolute curvature, followed by volume decreasing it, and finally, the relative curvature.

This expression can be generalized for any shape $f(t)$ with a unitary peak, period, and volume V_u, where the discharge hydrograph equals this shape rescaled based on the actual peak and period, where $Q(t) = Q_p f(t')$ and $t' = t/T$. The total volume is rescaled as $V = Q_p T V_u$. The temporal discharge curvature of $Q(t)$ is also rescaled from $f(t)$ as a function of the peak and period or volume (see Supporting Information S1):

$$\frac{\partial^2 Q}{\partial t^2} = \frac{Q_p}{T^2}\frac{\partial^2 f(t')}{\partial t^2}$$

or

$$\frac{\partial^2 Q}{\partial t^2} = \frac{{Q_p}^3}{V^2}{V_u}^2\frac{\partial^2 f(t')}{\partial t^2} \tag{14}$$

and the relative curvature can be expressed as:

$$C' = -\frac{\partial^2 f}{\partial t^2}{V_u}^2 \tag{15}$$

Thus, the curvature and diffusion of a flood wave with constant volume is much more sensitive to peak discharge Q_p (cubic exponent) compared with the case of constant period/length/frequency that shows a linear exponent. Flood waves are usually formed by water added to the river system (Dingman, 2009) such as the runoff produced by precipitation or reservoir releases due to dam break. Thus, assuming a flood wave has constant volume with variable period/length is the most realistic choice. Other types of waves as small flow perturbations may travel and attenuate keeping constant period/length but variable volume, but such approximation is not reasonable for floods.

The range of C' values can be evaluated for well-known continuous functions using Equation 15 (see Supporting Information S1). For instance, symmetric shapes present relative curvatures, such as $C' = \pi^2 = 9.87$ for ellipsoidal, $C' = 2\pi$ for Gaussian, $C' = \pi^2/2 = 4.93$ for sinusoidal, $C' = 32/9 = 3.56$ for parabolic, and $C' = 0$ for square functions. For curves that emulate natural hydrographs, the relative curvature increases as a function of the asymmetry, such as the NERC (1975) synthetic hydrograph $Q = Q_p\left[t/T_{rise}e^{1-t/T_{rise}}\right]^m$ with $C' = \frac{m}{s^2}$ and $C' \approx 5.78s^{-0.33}$, and the unit response function of the diffusive wave model, where $C' \approx 2\pi s^{-0.5}$ and $C' = 2\pi$ (Gaussian shape) for developed hydrographs. Finally, the relative curvature can also be easily estimated from an observed hydrograph, as $C' = -\frac{V^2}{{Q_p}^3}\frac{\partial^2 Q}{\partial t^2}$, by first calculating its volume, peak, and curvature.

2.6. Peak Attenuation Along the Flood Wave Trajectory

The diffusion wave model (Equation 1) can be expressed as the change in discharge along the flood wave trajectory using the definition of the substantial derivative (Brutsaert, 2005) as $\frac{D()}{Dt} = \frac{\partial()}{\partial t} + c\frac{\partial()}{\partial x}$ and:

$$\frac{DQ}{Dt} = D_h \frac{\partial^2 Q}{\partial x^2} \tag{16}$$

If the advection effects prevail over diffusion, then the spatial curvature is approximated as $\frac{\partial^2 Q}{\partial x^2} = \frac{1}{c^2}\frac{\partial^2 Q}{\partial t^2}$ obtained from Equation 1. Additionally, to predict the discharge peak along the flood wave trajectory, time t is substituted by the distance x as an independent variable of the model. Considering that $dt = dx/c$, the model becomes:

$$\frac{dQ_p}{dx} = \frac{D_h}{c^3}\frac{\partial^2 Q}{\partial t^2} \tag{17}$$

The use of such expression for flood peak estimation was also discussed by Lighthill and Whitham (1955), but they proposed to solve it by numerical methods, keeping the right-hand side constant. However, if $\frac{D_h}{c^3}\frac{\partial^2 Q}{\partial t^2}$ it is expressed as a function of Q_p, Equation 17 can be easily solved analytically as an ordinary differential equation to determine the peak discharge $Q_p(x)$ as a function of distance x. Analyses from previous sections show that D_h, c, and $\frac{\partial^2 Q}{\partial t^2}$ can all be expressed as potential functions of Q_p (e.g., Equations 3, 5, and 13), and consequently the decay of peak discharge in space can be parameterized as:

$$\frac{dQ_p}{dx} = -k{Q_p}^b \tag{18}$$

where k is interpreted as a decay factor, and the exponent b expresses the nonlinearity of peak discharge attenuation. This ordinary differential equation can be solved by separation of variables and simple integration:

$$\int_{Q0}^{Q(x)} \frac{1}{{Q_p}^b} dQ_p = \int_0^x k\, dx \tag{19}$$

resulting in:

$$\frac{Q(x)}{Q_0} = \frac{1}{\left[1 + (b-1)\, k\, Q_0^{b-1}\, x\right]^{\frac{1}{b-1}}} \tag{20}$$

where $\frac{Q(x)}{Q_0}$ is the attenuated relative peak discharge that decreases along the flood wave trajectory x according to a power function (see Figure 1d). Notice that the subscript p was suppressed for simplicity. The shape of this decay function relates to the exponent b, and it is scaled by the parameters k and b but also the initial peak discharge Q_0 at $x = 0$. The degree of nonlinearity and the importance of the initial discharge Q_0 vanishes as b approaches 1. The model is linear, and the decay is exponential for $b = 1$:

$$\frac{Q(x)}{Q_0} = e^{-kx} \tag{21}$$

The third case is when $b = 0$, for which the discharge changes at a constant rate k, expressed as $\frac{Q(x)}{Q0} = 1 - kx$.

If the curvature of the discharge hydrograph is parametrized assuming constant flood wave volume (Equation 13), and accounting for floodplain storage (Equations 7 and 8), then the diffusion model from expression 7 becomes:

$$\frac{dQ_p}{dx} = -D_h\left(\frac{w_t}{w}\right)^2 C' \frac{{Q_p}^3}{c^3 V^2} \tag{22}$$

indicating that nonlinearity is incorporated in the peak attenuation (cubic exponent). Hydraulic diffusivity and celerity may also change with discharge along the flood wave trajectory. They can be expressed from Equations 3 and 5 as a function of the initial values, computed from the peak flow Q_0 at $x = 0$:

$$\begin{aligned} D_h &= D_{h0}(\,Q/Q_0\,) \\ c &= c_0(\,Q/Q_0\,)^{1-1/\beta} \end{aligned} \tag{23}$$

and Equation 22 is rewritten with constant initial parameters to represent the change in peak discharge with distance:

$$\frac{dQ}{dx} = -D_{h0}\left(\frac{w_t}{w}\right)^2 C' \frac{Q_0{}^{2-3/\beta}}{c_0{}^3 V^2} Q^{1+3/\beta} \tag{24}$$

Thus, variable D_h increases the nonlinearity, while variable c decreases it as a function of the discharge rating β. If floodplain width is allowed to increase with discharge, nonlinearity can increase. This ordinary differential equation can be solved, as in Equations 19 and 20. After a few algebraic manipulations, the attenuated relative peak discharge $\frac{Q(x)}{Q_0}$ along the flood wave trajectory x is expressed as:

$$\frac{Q(x)}{Q_0} = \frac{1}{[1+\varphi x]^{\beta/3}} \tag{25}$$

This equation describes peak discharge decreasing along the distance x according to a power function (see Figure 1d), with an exponent related to the flow rating exponent β and distance scaled by φ, defined as the flood peak attenuation factor. Larger β and φ values cause larger attenuation rates.

2.7. Flood Peak Attenuation Factor

The flood peak attenuation factor φ [L^{-1}] is defined (from Equations 19, 24 and 25) as:

$$\varphi = \frac{3}{\beta}\frac{D_{h0}}{c_0{}^3}\left(\frac{w_t}{w}\right)^2 C' \frac{Q_0^2}{V^2} \tag{26}$$

Analyses of the parameter exponents show that attenuation increases mostly with floodplain storage $\left(\frac{w_t}{w}\right)$ and initial peak discharge Q_0 but also with hydraulic diffusivity D_{h0} and hydrograph relative curvature C'. It decreases mostly with celerity c_0, then with hydrograph volume V and flow rating exponent β.

For natural rivers using the empirical parameterizations of Equation 6 and $\beta = 5/3$, and Equations 3 and 26, the flood peak attenuation factor is expressed as:

$$\varphi = 0.1944\frac{n^{1.8} w^{0.2}(1-v^2)}{S^{1.9}}\left(\frac{w_t}{w}\right)^2 C' \frac{Q_0^{1.8}}{V^2} \tag{27}$$

revealing by the exponents that floodplain storage plays a larger role than river active flow width w in increasing attenuation, along with a larger Manning's roughness and smaller river slope S.

The first part of the φ expression (e.g., $\frac{3}{\beta}\frac{D_{h0}}{c_0{}^3}\left(\frac{w_t}{w}\right)^2$) represents the channel flow hydrodynamic characteristics, where the large floodplain storage, hydraulic diffusivity, and small celerity enhance attenuation. The second part describes the inflow hydrograph ($C'\frac{Q_0^2}{V^2}$), showing that a larger initial peak discharge with a smaller volume and larger relative curvature increases attenuation.

These findings based on analytical reasoning of the diffusion wave model agree with and complement previous interpretations from numerical experiments and analyses of the Saint-Venant equations (e.g., Ponce et al., 2003; Rutschmann & Hager, 1996).

2.8. Case of Small Amplitude Flood Wave Over Large Reference Flow

A common alternative case is a flood wave consisting of a small discharge change ΔQ with volume V moving over a reference discharge. In this case, the celerity and hydraulic diffusivity parameters for the reference discharge are assumed constant. Following similar reasoning from previous sections, the model is adapted:

$$\begin{aligned}\frac{\Delta Q(x)}{\Delta Q_0} &= \frac{1}{[1+\varphi x]^{0.5}} \\ \varphi &= 2\frac{D_{h0}}{c_0{}^3} C' \frac{\Delta Q_0^2}{V^2}\end{aligned} \tag{28}$$

The unit impulse function of the linear diffusive wave model (Brutsaert, 2005; Dooge, 1973) is built assuming a unitary volume input that is conserved while it propagates downstream. As it shares the same fundamental assumptions with Equation 28, they should provide similar predictions. For a given volume V, the impulse function is:

$$Q(x,t) = V\frac{x}{\sqrt{4\pi D_{h_0} t^3}} e^{-\frac{(x-c_0 t)^2}{4D_{h_0} t}} \tag{29}$$

Except for small x, the discharge peak occurs at $t = x/c_0$, and the expression for the peak along a given distance is:

$$Q_p(x) = \frac{V}{\sqrt{4\pi \frac{D_{h0}}{{c_0}^3} x}} \tag{30}$$

For $x \to 0$, then $Q_0 \to \infty$, and this expression is not practical for estimating $\frac{Q(x)}{Q_0}$. However, it is convenient to assume that Q_0 relates to peak discharge at an initial distance $x_0 > 0$ and change the coordinates to $x' = x + x_0$, so x' refers to a distance downstream of x_0. After applying it to Equation 30, the attenuated relative peak discharge is:

$$\frac{Q(x)}{Q_0} = \sqrt{\frac{x_0}{x}} = \sqrt{\frac{x_0}{1 + x'/x_0}} = \frac{1}{\left(1 + 4\pi \frac{D_{h0}}{{c_0}^3} \frac{Q_0^2}{V^2} x'\right)^{0.5}} \tag{31}$$

The result is the same as that predicted in Equation 28 using the specific relative curvature of $C' = 2\pi$ for the unit impulse function, thus supporting the arguments developed herein.

2.9. Case of Small Flow Perturbation With Constant Parameters

A second alternative case is a wave consisting of a small flow perturbation with amplitude Q' that attenuates while keeping its period and length constant, but attenuating its volume. Considering the common assumptions of constant parameters and the curvature of a sinusoidal wave (Section 2.5), then the diffusive wave model is:

$$\frac{dQ'}{dx} = -\frac{2\pi^2 D_{h0}}{c_0^3 T^2} Q' \tag{32}$$

After integration, the amplitude of the perturbation attenuates exponentially, with a constant attenuation factor that is independent of the initial conditions:

$$\begin{aligned} \frac{Q'(x)}{Q'_0} &= e^{-\varphi x} \\ \varphi &= \frac{2\pi^2 D_{h0}}{c_0^3 T^2} \end{aligned} \tag{33}$$

This result is similar to the expressions that show an exponential decay of flow perturbations, which are obtained using harmonic and small perturbation linear analyses (e.g., Fenton, 2019; Kundzewicz & Dooge, 1989; Ponce et al., 2003; Ponce & Simons, 1977), and the result is almost equal to that obtained by Ponce et al. (1996). All these approximations assume either constant wavelength and period and/or a predefined function. The result is also similar to V. P. Singh et al. (1998), who found an exponential decay for the flood peak after assuming constant hydrograph absolute curvature at the peak, which was based on observations. Although these expressions are all analogous, their fundamental hypothesis, that is, constant wave curvature or length/period, may not be realistic for representing flood wave attenuation. This is because flood waves usually conserve the added mass of water to the system (Dingman, 2009) by increasing its length/period and decreasing its curvature.

2.10. Flood Peak Attenuation Length

The flood attenuation model (Equation 25) can also be interpreted using a practical indicator related to the distance necessary to attenuate an input hydrograph. The flood peak attenuation length $L_{1/n}$ is defined here as the distance along the flood wave trajectory travel path in which discharge decreased by the factor $1/n$:

$$L_{1/n} = \frac{n^{3/\beta} - 1}{\varphi} \tag{34}$$

For example, the river distance (in kilometers) that is necessary for the discharge to reduce by half of the initial value in natural rivers, and assuming SI units, is:

$$L_{1/2} = \frac{0.00248}{\varphi} \tag{35}$$

Attenuation length $L_{1/n}$ is inversely proportional to the attenuation factor φ, and the above interpretations for φ are easily extended to $L_{1/n}$. For instance, the floodplain storage decreases the attenuation length by the factor $\left(\frac{w_f}{w}\right)^2$.

2.11. Flood Peak Attenuation With Variable Parameters

Natural rivers often have variable topography and lateral inflows, and the attenuation factor φ can also vary along the flood wave travel path. In such cases, the attenuation model can easily be adapted by applying it recursively along segments of length Δx_i, where φ_i is assumed constant:

$$\frac{Q(x)}{Q_0} = \prod_i \frac{1}{[1 + \varphi_i \Delta x_i]^{\beta/3}} \tag{36}$$

3. Sensitivity Analyses and Validation Against Numerical Modeling

The flood attenuation model was applied in 20 scenarios covering a wide range of river characteristics and flow conditions commonly found in nature. This assessment represents a sensitivity analysis of the governing factors in flood peak attenuation, as well as a validation of the model. For the latter, our results were compared with numerical simulations solving the Saint-Venant equations using the popular HEC-RAS hydrodynamic model (USACE, 2020).

3.1. Methods

Model scenarios (Figure 2) were built from a reference (Ref) and each of the model input parameters were decreased and increased (indicated by "−" and "+" symbols) over a reasonable range. The case of natural rivers with rectangular cross section was evaluated. The reference scenario (Ref) consists of a medium size river with width w = 50m. According to estimates performed by Moody and Troutman (2002), widths of rivers across the globe vary around 3x for a similar bankfull discharge, so we assumed $w-$ = 15m and $w+$ = 150 m. According to the same estimates, bankfull discharge for a river width of 50 m is approximately 50 m^3/s. Growth curves from regional flood frequency analyses (e.g., Rosbjerg et al., 2013; Smith et al., 2015) show that flood discharges for 10, 100, and 1,000 year return periods are approximately 2x, 1.5–6x, and 1.5–30x larger than the mean annual flood, respectively. We evaluated flood peak discharges that are representative of a large flood (~100 years, Q_0 = 250 m^3/s), an extreme flood (>1,000 years or dam break, Q_0+ = 5,000 m^3/s), and a moderate flood (~10 years, Q_0- = 100 m^3/s). Hydrograph volume was selected assuming base times representative of rapid (2 hr and $V-$ = 0.9 hm^3), moderate (12 hr, V = 5.4 hm^3) and slow (1 week, $V-$ = 75.6 hm^3) cases. Varying both the initial discharge and volume but keeping base time constant was also assessed ($Q_0 - V-$ and $Q_0 + V+$). River slope was assumed as S = 1 m/km for moderate-slope, $S-$ = 10 cm/km for low-slope, and $S+$ = 50 m/km for steep rivers, which agrees with the ranges shown by Frasson et al. (2019) for global rivers. Floodplain storage was $\left(\frac{w_f}{w}\right)$ = 3 for average rivers (Ref), $\left(\frac{w_f}{w}\right)-$ = 1 for rivers with no floodplains, and $\left(\frac{w_f}{w}\right)+$ = 10 for floodplain-dominated rivers (e.g., similar to the Amazon River). The Manning roughness coefficient can also vary (Chow, 1959), exhibiting n = 0.035 for natural streams, $n-$ = 0.015 for built channels, and $n+$ = 0.08 for rough streams. The reference scenario assumed an asymmetric hydrograph with s = 0.4 as an approximation of natural cases, and a steep ($s-$ = 0.1) and symmetric $s+$ = 1 hydrograph was also evaluated. The model was applied using equations presented in Section 2, assuming a natural river with a rectangular cross-section. The relative curvature was modeled as $C' = 3\pi s^{-0.5}$, and as $C'- = 5.78 s^{-0.33}$ in an additional scenario. The interaction between parameters were examined by perturbing them all together to increase (All+) and decrease (All−) attenuation using mid values between Ref and + or—scenarios. All the other variables and flood peak attenuation were computed using the equations provided in Section 2 and a simple spreadsheet (available at https://data.mendeley.com/datasets/pjkmzh8tf8/1).

10.1029/2023WR034692

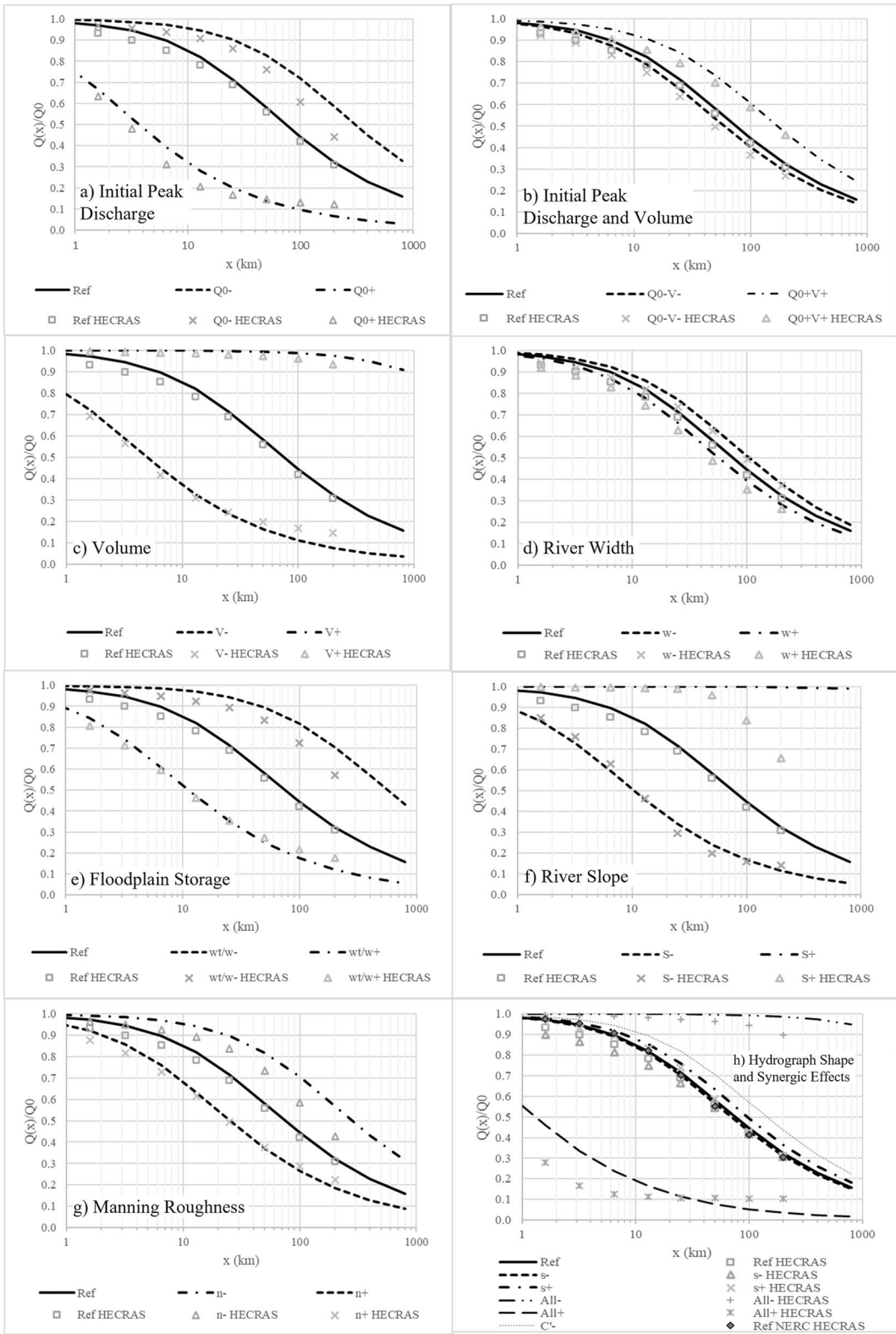

Figure 2.

The selected scenarios cover a wide range of flood wave and flow characteristics. Flood wave celerity ranges from 0.4 to 8 m/s, which agrees with what is found in the literature (e.g., Allen et al., 2018; Meyer et al., 2018; T. H. Wong & Laurenson, 1983). Froude numbers range from 0.1 to 0.7, representing subcritical flows found in natural rivers. Flood wave types include kinematic, diffusive, and dynamic waves, according to Moussa and Bocquillon (1996) criteria. And flood peak attenuation lengths range from a few to more than thousands of kilometers.

The scenarios were also evaluated using numerical simulations, solving the Saint-Venant equations using the HEC-RAS 1D hydrodynamic model (USACE, 2020). The finite volume Preissmann's scheme was adopted ($\theta = 1$ for the implication parameter). River cross-sections were discretized into 1 cm height intervals. Floodplains were assumed as storage areas by adopting high Manning's coefficient values (50). Upstream boundary conditions were set as triangular hydrographs and one case of an equivalent smoothed NERC hydrograph was used. Normal depth was adopted at the downstream boundary. A baseflow equal to 10% flood peak was added to the hydrograph to avoid numerical instabilities related to the dry bed. Reaches long enough to observe significant flood attenuation with length of 200 km were discretized every 100 m following Castellarin et al. (2009) criteria to avoid numerical diffusion, and the simulation time interval was set as variable, with a Courant number lower than 0.7, to avoid numerical instabilities. Numerical issues were verified by interpreting hydrographs, and the volume errors were less than 0.0028% in all cases.

3.2. Results

The sensitivity analyses (Figure 2) demonstrate that flood peak attenuation with distance x is governed mostly by initial peak discharge, hydrograph volume, floodplain storage, and river slope. For instance, changing these input variables impacted attenuation lengths ($L_{1/2} \approx 65$ km, Ref) by orders of magnitude, from less than 10 km to more than 300 km. The relative peak discharge $\frac{Q(x)}{Q_0}$ varied from less than 0.2 to 1 when it is 0.5 for the reference scenario. On the other hand, the river width and hydrograph shape presented a minor influence over the attenuation, impacting relative peak discharge by around 0.1. These findings agree with the interpretations of the role of the input variables on attenuation using analytical reasoning from Section 2.7.

Predictions obtained from the flood attenuation model are similar to the results obtained from numerical simulations using the HEC-RAS model. Differences in predicted relative peak discharge $\frac{Q(x)}{Q_0}$ are generally less than 0.1, thus much smaller than its variability along the distance x or caused by different river characteristics and flow conditions. It is smaller than typical errors of flood discharge observations (from 5% to more than 40%, Fleischmann et al., 2019; McMillan et al., 2012). Also, mean absolute difference between attenuation lengths computed by the hydrodynamic and simplified model are 19%. Such agreement demonstrates the validity and accuracy of the proposed model in the context of practical applications.

The flood wave attenuation model is sensitive to initial peak discharge in the case where the hydrograph volume is constant and the period is variable (Figure 2a), as it impacts hydrograph absolute curvature (Equation 13), increasing attenuation. On the other hand, the model sensitivity is much lower when initial peak discharge changes with constant period and variable volume (Figure 2b), and the result is the opposite as celerity increases with discharge, thus reducing the attenuation. Increasing hydrograph volume and period has a considerable impact on decreasing the attenuation of flood peak discharge (Figure 2c).

River width (Figure 2d) has a minor effect on attenuation compared with floodplain storage relative size (Figure 2e), which increases attenuation, in agreement with the interpretation of exponents of Equation 27 ($w^{0.2}$ and $\left(\frac{w_f}{w}\right)^2$). The flood peak attenuation is largely influenced by the river slope (Figure 2f), as it governs flood wave celerity and hydraulic diffusivity. Low river slopes decrease celerity and increase hydraulic diffusivity, thus increasing attenuation. In this particular case, correcting flood wave celerity for the looped rating curve (Section 2.4) is especially important because the rapidly varying flood wave changes the surface water slope and

Figure 2. Sensitivity analyses and validation of the flood attenuation model (lines) using a numerical solution of Saint-Venant equations from the HEC-RAS hydrodynamic model (markers). Attenuated relative peak discharge $\frac{Q(x)}{Q_0}$ along the flood wave trajectory x for the reference (Ref) scenario and decreased ("−") and increased ("+") parameter values, (a) varying the initial peak discharge while keeping volume constant, (b) varying the initial peak discharge and volume while keeping base time constant, varying (c) hydrograph volume, (d) river width, (e) floodplain storage, (f) river slope, (g) Manning's roughness coefficient, and (h) hydrograph shape in terms of asymmetry and estimate of relative curvature and also evaluating synergic effects varying all parameters together.

increases celerity (~150% for scenario $S-$), decreasing the attenuation. For large river slopes, celerity is large and hydraulic diffusivity vanishes resulting in small or null attenuation. In $S+$ scenario, differences were observed at larger distances. The larger attenuation of the numerical simulation was caused by an expressive steepening of the hydrograph, often referred to as kinematic shock (Lighthill & Whitham, 1955), which is rarely found in nature (Ponce, 1991b). Increasing Manning's roughness coefficient increased attenuation (Figure 2g), but this parameter exhibited smaller effects on attenuation compared to others.

The hydrograph shape exhibited smaller effects on attenuation (Figure 2h). Varying hydrograph asymmetry impacts relative peak discharge by less than 0.1, and numerical modeling results converge for large distances. This is likely because the symmetric input hydrograph ($s+$) steepened because of nonlinear celerity effects and the steeper hydrograph ($s-$) flattened because of diffusion effects (as discussed in Ponce (1991a) and Collischonn et al. (2017)). Differences between the HEC-RAS simulations using a triangular hydrograph shape and an equivalent smoother NERC hydrograph are also small. The model for estimating relative curvature C' in the simulations provides unbiased results for the Ref scenario, but when using an alternative estimative ($C'-$), the differences are smaller than the discharge peak variability with distance or changing the other input variables. Finally, synergic effects caused by mid variations of all parameters together (Figure 2h) can cause larger impacts on attenuation if compared to large variations of single parameters.

4. Validation Against Historical Dam-Break Floods

The flood attenuation model was also validated against 29 observations of flood peak discharge from 11 dam breaks (Figure 3) documented in USBR (1989) and CPRM (2015) (data available at https://data.mendeley.com/datasets/pjkmzh8tf8/1). These past historical events represent a wide variety of flood wave characteristics and constitute a valuable set of independent observations for model validation. The observations contain dam-break data from water reservoirs (9) and mining tailing dams (2), with small to large volumes (0.5–310 hm^3). The data include hydrographs with a small to large period, rising times, and peak flows (30 min–1 day, 15 min to 6 hr, and ~680 to 65,000 m^3/s), traveling over a variety of reach lengths (4–342 km) in canyon valleys and meandering rivers with floodplains, with both high and low slopes (0.5–18 m/km), with small to very large widths of main channel active flow (10–800 m) and floodplain inactive storage (1x to 50x river width). The observations include the recent 2015 Fundão dam-break disaster that impacted Rio Doce in Brazil and events that served as test cases for past flood wave modeling research, such as Teton in 1976 and Buffalo Creek in 1972 (e.g., Wetmore & Fread, 1981).

4.1. Methods

Observations of flood wave peak flow and celerity and reservoir storage were obtained from the compilation provided by USBR (1989), except for Fundão Dam/Doce River, where CPRM (2015) data were used. The inflow hydrograph volume was estimated as being equal to the reservoir storage. The time of rise was assumed equal to the dam breach formation/development times compiled by Wahl (1998). High-resolution satellite imagery (<meters) was used to support the digitalization of river centerlines using Google Earth Pro software covering the locations described in USBR (1989) and CPRM (2015). It was also used to measure reach and floodplain lengths, slopes based on SRTM DEM (30 m spatial resolution, ~5 m vertical error), and river and floodplain widths (average of 4–5 per reach, see river centerlines and cross-sections in Figures S1–S11 of Supporting Information S1 and https://data.mendeley.com/datasets/pjkmzh8tf8/1), also supported by descriptions from USBR (1989) and damfailures.org. The Manning coefficient was assumed constant (0.035) for all cases. All the other variables and flood peak attenuation were computed using the equations provided in Section 2 and a simple spreadsheet (available at https://data.mendeley.com/datasets/pjkmzh8tf8/1). The performance of the model was also compared with the empirical model $\frac{Q(x)}{Q0} = 10^{-0.0125x}$ proposed by USBR (1989), which estimates flood peak attenuation as a function of river distance only and represents a simplified approach that is currently used for dam-break assessments.

4.2. Results

The analyses reveal a large spread of observed flood peak attenuation and show that river distance x alone does not explain such variability (Figure 3a). Predictions from the flood attenuation model can approximate the

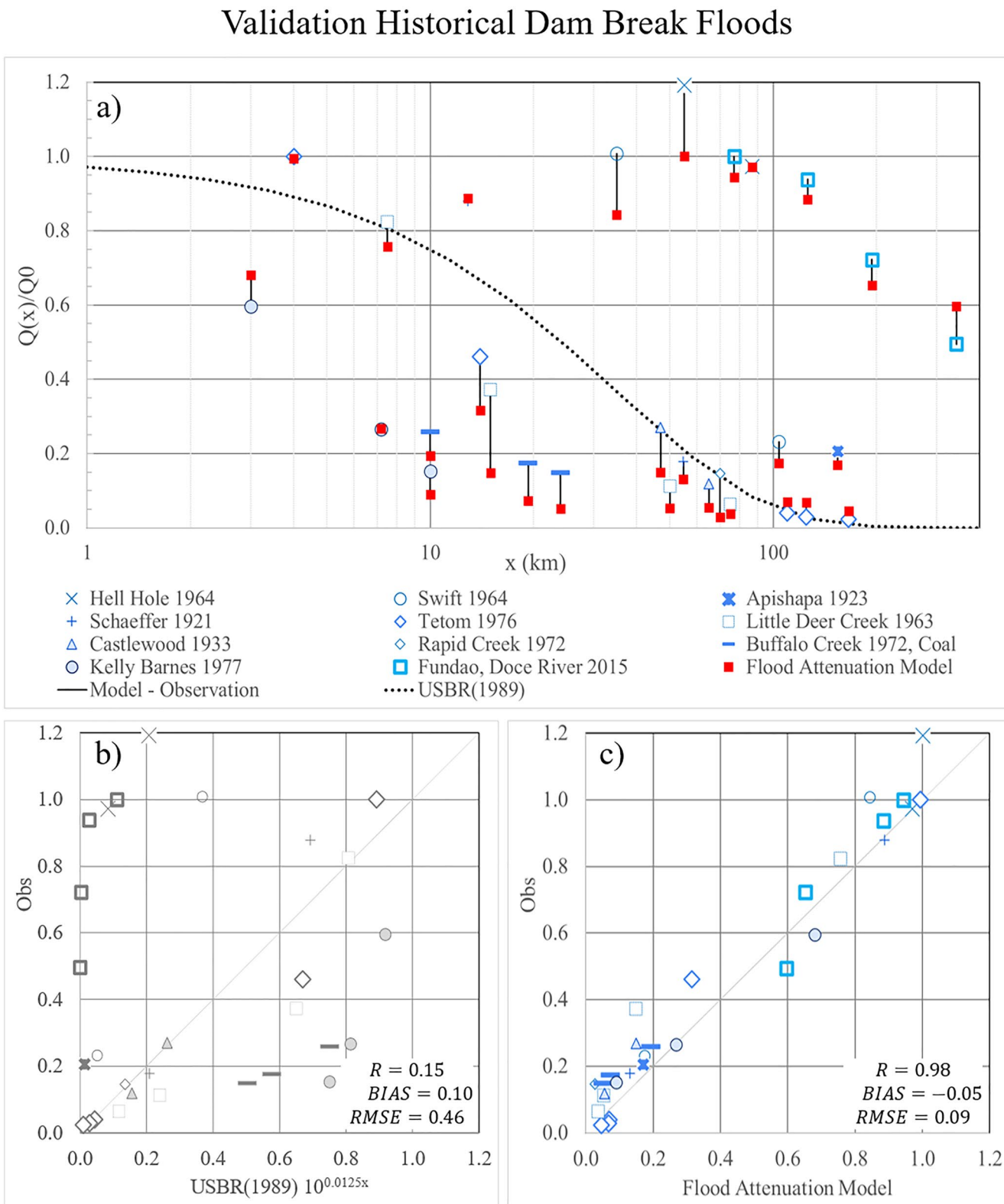

Figure 3. Validation of flood attenuation model against observations from 11 historical dam breaks. (a) Relative peak discharge as a function of river distance for the flood attenuation model (red markers), observations (blue markers), differences (black line), and estimates based on distance only from USBR (1989) (black dashed line). Scatterplots showing relative peak discharge from model estimates versus observed and performance metrics for the USBR (1989) (b, gray) and Flood Attenuation Model (c, blue).

historical observations of relative peak discharge and reproduce its variability. For instance, estimated attenuation lengths for the different river reaches range from a few to thousands of kilometers. The model validity is corroborated by the satisfactory values of the performance metrics, such as the coefficient of correlation, bias, and root mean squared error ($R = 0.98$, $BIAS = -0.05$, and $RMSE = 0.09$). The correlation coefficient computed between downstream relative peak discharge and the input parameters show larger values for floodplain storage $\left(\frac{w_t}{w}\right)$ ($R = -0.60$). As the errors of some of the input parameters may corrupt model estimates, floodplain storage $\left(\frac{w_t}{w}\right)$ was selected for simple verification. Its values were perturbed using a large and conservative uncertainty range (−50% and +100%), but the model performance metrics are satisfactory ($R = 0.96$ and $RMSE = 0.18$). Estimated flood wave celerity also agrees with 10 historical estimate values, with $R = 0.79$ and a median absolute error of 58%. The model accuracy for relative peak discharge is markedly improved compared to estimates based on distance only ($R = 0.15$, $BIAS = 0.10$, and $RMSE = 0.46$). Finally, the model performance also satisfies the requirements for the river hydrodynamic predictions to be considered locally relevant (Fleischmann et al., 2019). For example, *RMSE* is lower than typical discharge observation uncertainty (5% to more than 40%).

The model validation against this set of historical events supports the proposed representation of the flood wave and solution of the hydrodynamic equations. It is also a proof of concept showing that this model is suitable for first assessments of attenuated flood peak discharge, such as dam-break applications, since it is accurate and can be easily implemented using simple spreadsheets and a few parameters extracted with GIS methods.

5. Validation Against Observed Natural Floods

The flood attenuation model was also validated against 15 paired observations of natural flood hydrographs at seven large Brazilian rivers (Figure 4) (data available at https://data.mendeley.com/datasets/pjkmzh8tf8/1). This sample of river reaches was selected following Meyer et al. (2018) given the availability of paired in situ gauges with small incremental drainage area or mean flow, in order to avoid a potential influence of lateral inflows over observed flood peaks. It covers a variety of river and flood wave characteristics, including fast and seasonal floods (2 days–2 months), over different reach lengths (58–658 km), straight and meandering rivers with low to mid slopes (0.1–0.5 m/km), with small to very large widths of main channel active flow (50 m–1 km) and floodplain inactive storage (1x to 20x river width).

5.1. Methods

Observed discharge hydrographs at in situ gauges were obtained at hourly and daily time steps from the Brazilian Water Resources Agency (https://www.snirh.gov.br/hidrotelemetria/) and CAMELS-BR data set (Chagas et al., 2020a), respectively. Lateral inflows effects were minimized from downstream discharge by correcting it by the ratio of mean upstream and downstream values computed for the period of analyses. For each river, the hydrograph of 1–3 flood events were selected and peak discharge, time of rise, duration and volume were estimated. High-resolution satellite imagery was used to support the digitalization of river centerlines using Google Earth Pro software covering the river reach from upstream to downstream gauges. It was also used to measure reach and floodplain lengths, slope, and river and floodplain widths (average of 3–5 per reach, see river centerlines and cross-sections in Figures S13–S19 in Supporting Information S1). The Manning coefficient was assumed constant (0.035) for all cases. All the other variables and flood peak attenuation were computed using the equations provided in Section 2 and a simple spreadsheet (all parameters and calculations are available at https://data.mendeley.com/datasets/pjkmzh8tf8/1).

5.2. Results

The analyses expose different behaviors concerning flood hydrograph attenuation. For instance, Iguaçu, Araguaia and Aquidauana Rivers present low flood peak changes, while downstream hydrographs are very attenuated at Cuiabá, Miranda and São Francisco Rivers (Figure 4a). Observations show that reach lengths alone do not explain such variability (Figure 4c) that are governed mostly by river slope and floodplains. Some of these natural hydrographs present complex shape, for instance with multiple peaks. Even so, estimates from the flood attenuation model reproduce observations of downstream peak discharge (Figure 4a) and relative peak discharge (Figure 4b) as shown by the satisfactory values of the performance metrics ($R = 0.88$, $BIAS = 0.00$, and $RMSE = 0.09$).

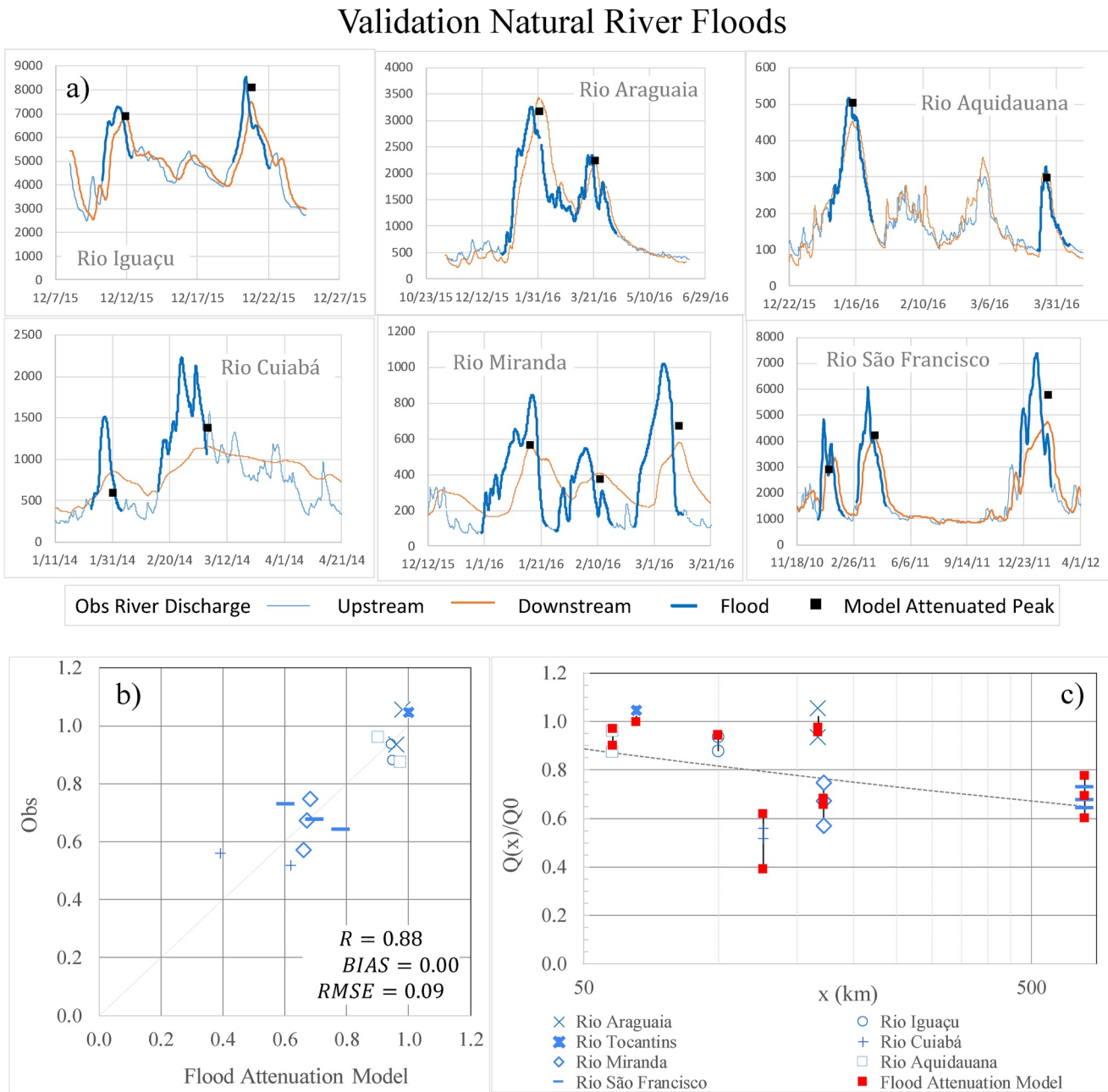

Figure 4. Validation of flood attenuation model against observations from 15 natural floods at seven large rivers. (a) Discharge hydrographs (m^3/s) observed at upstream (blue) and downstream (orange) in situ gauge stations, accessed flood events (bold blue) and predicted attenuated flood peak (black square). (b) Scatterplots showing relative peak discharge from flood attenuation model versus observed and performance metrics. (c) Relative peak discharge as a function of river distance for the flood attenuation model (red markers), observations (blue markers), differences (black line), and estimates based on distance only (black dashed line).

Estimated flood wave celerity agrees with values based on observed peak times, with $R = 0.95$ and median absolute error of 56%. Variations in model's performance between rivers and flood events can be related to discharge corrections to remove lateral inflows, uncertainty in observations of flood flows, or some variability of parameters as floodplain width as discussed in Section 2.3.

The model can replicate the diverse flood attenuation found among the different rivers. This validation against this set of observed hydrographs of natural flood events supports the proposed representation of the flood wave and model's assumptions. It shows that this simple model is appropriated for studying the attenuation of natural river flood waves, since it is accurate even when fed by approximate parameters estimated with simple GIS methods.

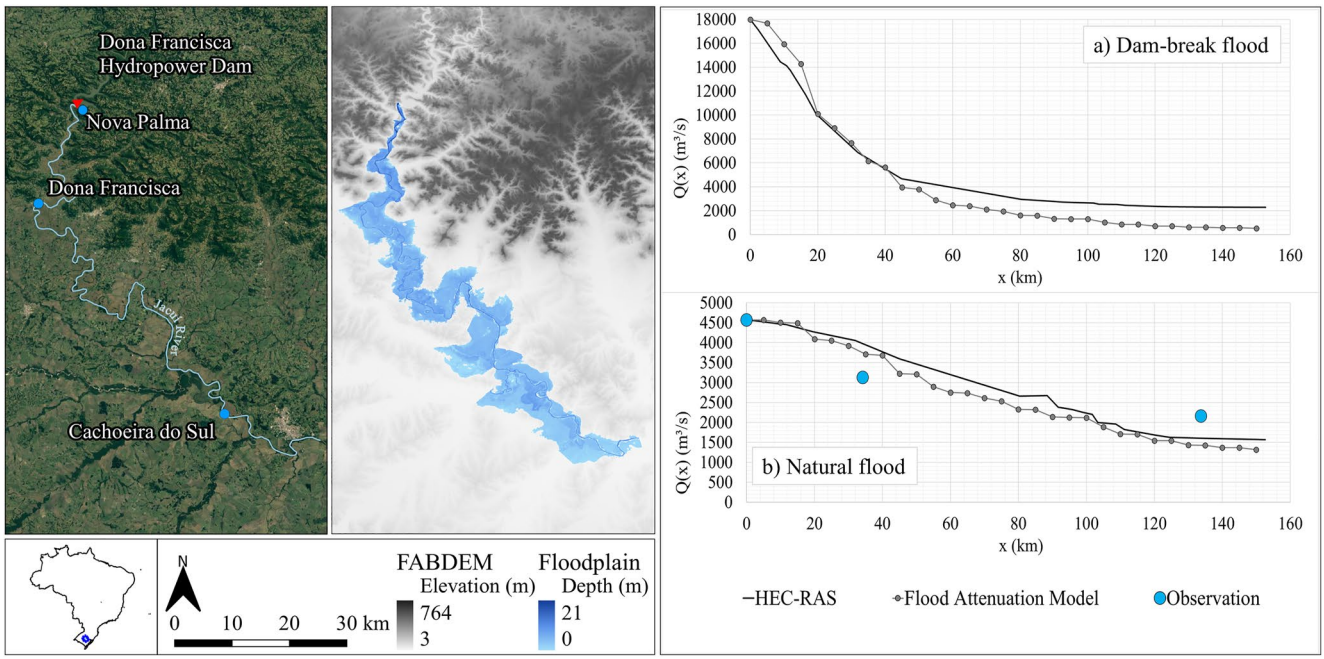

Figure 5. Comparison of the flood attenuation model over a complex terrain and a typical detailed hydrodynamic model (HEC-RAS) and observations. (a) Jacuí River in south Brazil between the Dona Francisca Dam (red) and Cachoeira do Sul, along with in situ gauging stations (blue), terrain from FABDEM (gray), and simulated flood inundation depth (blue field, HEC-RAS model). (b) Peak discharge along the flood wave path, estimated using the analytical flood attenuation model (gray markers), HEC-RAS (black line), and in situ observations (blue circles) for a hypothetical dam-break flood and the January 2010 natural flood.

6. Test Case in Complex Terrain

Finally, the flood attenuation model with variable parameters was assessed over a complex terrain by comparing it with in situ observations and results from a detailed hydrodynamic model, which is representative of current river modeling practices.

6.1. Methods

The Jacuí River was selected as a test case (Figure 5). It is located in south Brazil between Santa Maria and Porto Alegre cities. The portion of the Jacuí River between the Dona Francisca hydropower dam and Cachoeira do Sul city was studied (150 km). The river runs through a valley with a slope of ∼1 m/km and a small floodplain, and then over a reach of 10–20 cm/km with large floodplains (up to 100x the main river's width) covered by rice fields. The natural flood that occurred in January 2010 was evaluated. It raised the Jacuí River levels by more than 10 m, causing the collapse the main bridge of the region and important human/economic losses. In a second scenario, an extreme flood caused by the hypothetical Dona Francisca dam break is evaluated.

Inflow hydrographs for the natural flood event were obtained from the Reservoir Monitoring System—SAR of the Brazilian National Water Agency—ANA (ANA, 2013). Dam-break peak flow was estimated as a function of reservoir volume using the K. P. Singh and Snorrason (1984) equation. Downstream peak discharge observations for validation were obtained from ANA's gauging stations (https://www.snirh.gov.br/hidroweb/).

High-resolution satellite imagery was used to support the digitalization of the river centerline using Google Earth Pro software to measure reach lengths, slopes, and river and floodplain areas (see Figure S12 in Supporting Information S1). The flood attenuation model (Equation 36) was applied recursively on regular reaches of 5 km. Alternative discretization was also evaluated with segments of 10, 20, 50, and 150 km, and also irregular reaches ranging from 1 to 35 km, matching the ANA's official river network segmentation (ANA, 2017). Minimum slope of 0.1 m/km was assumed. All other variables and flood peak attenuation were computed using the equations provided in Section 2 and a simple spreadsheet (available at https://data.mendeley.com/datasets/pjkmzh8tf8/1).

The detailed hydrodynamic model was built using HEC-RAS software (USACE, 2020) with the 1D approximation and the FABDEM Digital Elevation Model at 30-m resolution (Hawker et al., 2022) informing channel

bathymetry and floodplain topography. As floodplains are covered by rice fields separated by levees and irrigation channels, they were modeled as storage areas using large Manning's roughness values (50). The volume errors related to numerical issues were less than 0.0063%. No calibration was performed for any of the models.

6.2. Results

Predictions of attenuated peak discharge along the river using the flood attenuation model and the detailed hydrodynamic model are equivalent (Figure 5b). In both models, attenuation is larger for the dam-break scenario, where initial peak discharge is larger, but the volume is smaller than the natural flood. These results agree with analyses from Sections 2 and 3. Sensitivity analyses (Figure S20 in Supporting Information S1) show that increasing discretization up to 5 km improves model realism but irregular discretization with smaller reaches can produce noise in results. Since the attenuation factor and the model are nonlinear, the reach lengths should be chosen carefully to be small enough to capture spatial variability, but large enough, so it is not corrupted by noise in parameter estimates. For instance, river slope estimated from digital elevation models may be impacted by elevation inaccuracies and post processing (e.g., hydro-conditioning, hydro-flattening). LeFavour and Alsdorf (2005) indicated that the minimum reach length RL necessary to estimate small slopes as $S_{\min}$ using a DEM with error σ is given by $RL = \frac{2\sigma}{S_{\min}}$. This issue may be relevant for low slope rivers (e.g., $S_{\min}$ < m/km), where necessary reach lengths can be tens of km when using current global DEMs ($\sigma \sim$ meters). While full hydrodynamic models may adjust water surface and slope during simulation and accommodate part of slope errors, this issue cannot be neglected in the simplified model although part of it is also accounted in celerity corrections from Section 2.4. Even so, results from both the flood attenuation model and HEC-RAS agree with in situ observations of the peak discharge decreasing downstream. The differences between the model predictions also have the same order of magnitude of the model errors compared with the observations. Attenuation lengths of the flood wave are similar when estimated for observations (110 km), simple model (90 and 24 km) and hydrodynamic model (100 and 24 km) for both natural and dam-break scenarios (Figure 5). Results from this test case demonstrate that the proposed model can provide flood attenuation predictions that are equivalent to those provided by detailed hydrodynamic models typically used in practical applications.

7. Conclusions

Floods are the most common and damaging natural disaster, and flood waves have been studied for decades. Predicting how a flood wave peak attenuates while it propagates downstream is key for understanding the risks of natural and dam-break floods, for engineering design, reservoir operation, and environmental analysis. While current prediction tools involve the use of advanced computer simulations, there is still no popular simple model of flood wave peak attenuation. In this paper, a simple physically-based analytical model was developed for predicting the attenuation of flood wave peak discharge.

The flood attenuation model (Figure 1) represents the flood wave along its travel path, based on the diffusive wave with inertial effects approximation of Saint-Venant equations, while assuming a constant shape and volume of the hydrograph and wave profile. The proposed model accounts for variable celerity and hydraulic diffusivity, a generic discharge rating, floodplain storage, and looped rating curve effects.

According to the model, relative peak discharge decreases along the flood wave trajectory x according to a power function $\frac{Q(x)}{Q_0} = \frac{1}{[1+\varphi x]^{\beta/3}}$, with an exponent that is related to the flow rating β and distance x that is scaled by the attenuation factor $\varphi = \frac{3}{\beta}\frac{D_{h0}}{{c_0}^3}\left(\frac{w_t}{w}\right)^2 C'\frac{Q_0^2}{V^2}$. Parameters are related to the river hydrodynamic characteristics, such as hydraulic diffusivity D_{h0} (Equation 3), flood wave celerity c_0 (Sections 2.2 and 2.4), and floodplain storage $\left(\frac{w_t}{w}\right)$ (Section 2.3), and related to inflow hydrograph, such as initial peak discharge Q_0, hydrograph volume V, and its relative curvature C' (Section 2.5). Moreover, the model presents a practical indicator called the flood peak attenuation length $L_{1/n}$ informing the downstream distance in which discharge is decreased by the factor $1/n$ (e.g., $L_{1/2}[\text{km}] = 0.00248/\varphi$).

An alternative solution for the flood wave attenuation of a small discharge change over a reference value is consistent with the unit response function of the linear diffusive wave model, thus supporting the arguments developed herein. A second alternative solution for exponential attenuation that is independent of initial conditions was

found for small perturbation waves that attenuate while maintaining a constant period and length but attenuating its volume. This is analogous to previous analytical works, but such an approximation may not be realistic for flood waves since they usually conserve the added mass of water to the system.

Sensitivity analyses indicate that the main governing factors of flood wave attenuation are initial peak discharge and floodplain storage, which increase attenuation, and river slope and hydrograph volume, which decrease attenuation.

The model validity and accuracy were demonstrated using four different validation experiments. The proposed model replicated numerical solutions of the Saint-Venant equations for a wide range of river characteristics and flow conditions. It was accurate in reproducing 29 observations of attenuated peak discharge from 11 historical dam-break floods and considerably more accurate than a simplified empirical model. It also produced accurate attenuation of 15 natural floods over seven rivers with variable characteristics. Furthermore, it provided flood attenuation predictions that were equivalent to those provided by a detailed hydrodynamic model, representative of what is typically used in current flood modeling practice. The model errors were generally lower than 10% and not larger than the typical uncertainty of flood discharge observations. The multiple model validations also demonstrate its easy application. For instance, while parameters for the simple model were obtained within minutes and estimates are almost instantaneous over a simple spreadsheet, preparing and running a detailed HEC-RAS hydrodynamic model (Section 6) took a few workdays.

The present model may be inaccurate for specific cases when its basic hypotheses are violated and other hydrodynamic models should be preferred, as for complex systems with undefined 1D flow, complicated hydraulic structures or lateral inflows setup, strong backwater effects due to downstream controls, fast waves with large vertical accelerations, strong changes in hydrograph shape, transitions from free surface to pressurized flows, mud and debris flows with variable density or complex rheology. Even so, the proposed model covers a comprehensive range of floods found in nature.

The model validations support the proposed representation of the flood wave and solution of the hydrodynamic equations. Notably, it can be easily applied using simple spreadsheets (see example with technical description at https://data.mendeley.com/datasets/pjkmzh8tf8/1) and a few parameters extracted from current GIS databases. Recommended future work includes applying the model for practical applications such as first assessments of natural and dam-break floods, engineering design, and analyses of large river networks supported by remote sensing observations.

Data Availability Statement

All computations using the flood attenuation model were performed using simple spreadsheets provided at https://data.mendeley.com/datasets/pjkmzh8tf8/1 (Lima & Paiva, 2023). Hydrodynamic simulations were performed using HEC-RAS 6.3.1. from https://www.hec.usace.army.mil/software/hec-ras/download.aspx (USACE, 2020). Data from historical dam-break and natural floods are documented at https://data.mendeley.com/datasets/pjkmzh8tf8/1 (Lima & Paiva, 2023). River centerlines, river and floodplain cross sections and longitudinal profiles are Digitalized using Google Earth Pro (2023) software (https://earth.google.com/web/) and available at https://data.mendeley.com/datasets/pjkmzh8tf8/1 (Lima & Paiva, 2023). Discharge observations from Brazilian Water Agency ANA and CAMELS BR are available at https://www.snirh.gov.br/hidroweb/ (ANA, 2023b), https://www.snirh.gov.br/hidrotelemetria/ (ANA, 2023a) and https://zenodo.org/record/3964745 (Chagas et al., 2020b). Dona Francisca Reservoir volume and outflow are available at Reservoir Monitoring System—SAR of the Brazilian National Water Agency—ANA from https://www.ana.gov.br/sar/ (ANA, 2013). FABDEM data was obtained from https://data.bris.ac.uk/data/dataset/25wfy0f9ukoge2gs7a5mqpq2j7 (Hawker & Neal, 2021).

Acknowledgments
The authors are grateful for the financial support from Brazilian Water Agency ANA (Project Coorperação em Tecnologias para Análises Hidrológicas em Escala Nacional), CNPq (314543/2020-1) and CAPES (88887.646024/2021-00), and for the constructive comments and discussions from Alice Fassoni, Aline Meyer, Walter Collischonn, Arthur Tschiedel, Pedro Chaffe, Julian Eleutério, Eder Teixeira and Rute Ferla and also from P.-A. Garambois, two anonymous reviewers and the associate editor and the editor Hamid Moradkhani.

References

Allen, G. H., David, C. H., Andreadis, K. M., Hossain, F., & Famiglietti, J. S. (2018). Global estimates of river flow wave travel times and implications for low-latency satellite data. *Geophysical Research Letters*, *45*(15), 7551–7560. https://doi.org/10.1029/2018GL077914

ANA. (2013). Sistema acompanhamento de reservatórios – SAR. Retrieved from https://www.ana.gov.br/sar/

ANA. (2017). Base Hidrográfica Ottocodificada Multiescalas 2017 (BHO 2017). Retrieved from https://metadados.snirh.gov.br/geonetwork/srv/api/records/0c698205-6b59-48dc-8b5e-a58a5dfcc989

ANA - Brazilian National Water Agency. (2023a). HIDRO-Telemetria. Retrieved from https://www.snirh.gov.br/hidrotelemetria/

ANA - Brazilian National Water Agency. (2023b). HIDROWEB. Retrieved from http://www.snirh.gov.br/hidroweb

Arnold, J. G., Srinivasan, R., Muttiah, R. S., & Williams, J. R. (1998). Large area hydrologic modeling and assessment part I: Model development 1. *JAWRA Journal of the American Water Resources Association*, *34*(1), 73–89. https://doi.org/10.1111/j.1752-1688.1998.tb05961.x

Biancamaria, S., Lettenmaier, D. P., & Pavelsky, T. M. (2016). The SWOT mission and its capabilities for land hydrology. *Surveys in Geophysics*, *34*(2), 307–337. https://doi.org/10.17615/7e1v-tw69

Blöschl, G. (2022). Three hypotheses on changing river flood hazards. *Hydrology and Earth System Sciences*, *26*(19), 5015–5033. https://doi.org/10.5194/hess-26-5015-2022

Brunner, M. I., Slater, L., Tallaksen, L. M., & Clark, M. (2021). Challenges in modeling and predicting floods and droughts: A review. *Wiley Interdisciplinary Reviews: Water*, *8*(3), e1520. https://doi.org/10.1002/wat2.1520

Brutsaert, W. (2005). *Hydrology, an introduction* (p. 618). Cambridge University Press. https://doi.org/10.1017/CBO9780511808470

Buttinger-Kreuzhuber, A., Waser, J., Cornel, D., Horváth, Z., Konev, A., Wimmer, M. H., et al. (2022). Locally relevant high-resolution hydrodynamic modeling of river floods at the regional scale. *Water Resources Research*, *58*(7), e2021WR030820. https://doi.org/10.1029/2021WR030820

Castellarin, A., Di Baldassarre, G., Bates, P. D., & Brath, A. (2009). Optimal cross-sectional spacing in Preissmann scheme 1D hydrodynamic models. *Journal of Hydraulic Engineering*, *135*(2), 96–105. https://doi.org/10.1061/(ASCE)0733-9429(2009)135:2(96)

Chagas, V. B., Chaffe, P. L., Addor, N., Fan, F. M., Fleischmann, A. S., Paiva, R. C., & Siqueira, V. A. (2020a). CAMELS-BR: Hydrometeorological time series and landscape attributes for 897 catchments in Brazil. *Earth System Science Data*, *12*(3), 2075–2096. https://doi.org/10.5194/essd-12-2075-2020

Chagas, V. B., Chaffe, P. L., Addor, N., Fan, F. M., Fleischmann, A. S., Paiva, R. C., & Siqueira, V. A. (2020b). CAMELS-BR: Hydrometeorological time series and landscape attributes for 897 catchments in Brazil - Link to files. (1.1) [Dataset]. Zenodo. https://doi.org/10.5281/zenodo.3964745

Chanson, H. (2004). *Hydraulics of open channel flow*. Elsevier. https://doi.org/10.1016/B978-075065978-9/50024-6

Chow, V. T. (1959). *Open-channel hydraulics*. McGraw-Hill.

Chow, V. T., Maidment, D. R., & Mays, L. W. (1988). *Applied hydrology*. McGraw-Hill Book Company.

Collischonn, W., Fleischmann, A., Paiva, R. C., & Mejia, A. (2017). Hydraulic causes for basin hydrograph skewness. *Water Resources Research*, *53*(12), 10603–10618. https://doi.org/10.1002/2017WR021543

Costa, J. E. (1985). *Floods from dam failures* (Vol. 85). US Geological Survey. No. 560.

CPRM - SERVIÇO GEOLÓGICO DO BRASIL. (2015). *Monitoramento especial da bacia do Rio Doce. Relatório 01: Acompanhamento da onda de cheia*. CPRM. Retrieved from https://rigeo.cprm.gov.br/handle/doc/21587

Cunge, J. A. (1969). On the subject of a flood propagation computation method (Musklngum method). *Journal of Hydraulic Research*, *7*(2), 205–230. https://doi.org/10.1080/00221686909500264

Cunge, J. A., & Hager, W. H. (2015). Alexandre Preissmann: His scheme and his career. *Journal of Hydraulic Research*, *53*(4), 413–422. https://doi.org/10.1080/00221686.2015.1076894

David, C. H., Famiglietti, J. S., Yang, Z. L., Habets, F., & Maidment, D. R. (2016). A decade of RAPID—Reflections on the development of an open source geoscience code. *Earth and Space Science*, *3*(5), 226–244. https://doi.org/10.1002/2015EA000142

Dingman, S. L. (2009). *Fluvial hydraulics*. Oxford University Press.

Dooge, J. (1973). *Linear theory of hydrologic systems* (Vol. 1468). Agricultural Research Service, US Department of Agriculture.

Fenton, J. D. (2019). Flood routing methods. *Journal of Hydrology*, *570*, 251–264. https://doi.org/10.1016/j.jhydrol.2019.01.006

Fleischmann, A., Paiva, R., & Collischonn, W. (2019). Can regional to continental river hydrodynamic models be locally relevant? A cross-scale comparison. *Journal of Hydrology X*, *3*, 100027. https://doi.org/10.1016/j.hydroa.2019.100027

Fleischmann, A. S., Paiva, R. C., Collischonn, W., Sorribas, M. V., & Pontes, P. R. (2016). On river-floodplain interaction and hydrograph skewness. *Water Resources Research*, *52*(10), 7615–7630. https://doi.org/10.1002/2016WR019233

Frasson, R. P. D. M., Pavelsky, T. M., Fonstad, M. A., Durand, M. T., Allen, G. H., Schumann, G., et al. (2019). Global relationships between river width, slope, catchment area, meander wavelength, sinuosity, and discharge. *Geophysical Research Letters*, *46*(6), 3252–3262. https://doi.org/10.1029/2019GL082027

Getirana, A. C., & Paiva, R. C. (2013). Mapping large-scale river flow hydraulics in the Amazon Basin. *Water Resources Research*, *49*(5), 2437–2445. https://doi.org/10.1002/wrcr.20212

Google Earth Pro. (2023). The world's most detailed globe (Version 7.3.6.9345) [Software]. Google Earth Pro. Retrieved from http://www.google.com/earth/index.html

Hawker, L., & Neal, J. (2021). FABDEM V1-0. https://doi.org/10.5523/bris.25wfy0f9ukoge2gs7a5mqpq2j7

Hawker, L., Uhe, P., Paulo, L., Sosa, J., Savage, J., Sampson, C., & Neal, J. (2022). A 30 m global map of elevation with forests and buildings removed. *Environmental Research Letters*, *17*(2), 024016. https://doi.org/10.1088/1748-9326/ac4d4f

Hayami, S. (1951). *On the propagation of flood waves* (Vol. 1, pp. 1–16). Bulletins-Disaster Prevention Research Institute, Kyoto University.

Henderson, F. M. (1966). *Open channel flow*. MacMillan.

Hodges, B. R. (2013). Challenges in continental river dynamics. *Environmental Modelling & Software*, *50*, 16–20. https://doi.org/10.1016/j.envsoft.2013.08.010

ICOLD, C. I. G. B. (2022). *Dam Surveillance-Lessons Learnt from Case Histories: Bulletin 180*. Taylor & Francis Group.

Jarrett, R. D. (1984). Hydraulics of high-gradient streams. *Journal of hydraulic engineering*, *110*(11), 1519–1539. https://doi.org/10.1061/(asce)0733-9429(1984)110:11(1519)

Julien, P. Y., & Paris, A. (2010). Mean velocity of mudflows and debris flows. *Journal of Hydraulic Engineering*, *136*(9), 676–679. https://doi.org/10.1061/(asce)hy.1943-7900.0000224

Junk, W. J., Bayley, P. B., & Sparks, R. E. (1989). The flood pulse concept in river-floodplain systems. *Canadian Special Publication of Fisheries and Aquatic Sciences*, *106*(1), 110–127.

Koussis, A. D. (2009). Assessment and review of the hydraulics of storage flood routing 70 years after the presentation of the Muskingum method. *Hydrological Sciences Journal*, *54*(1), 43–61. https://doi.org/10.1623/hysj.54.1.43

Kundzewicz, Z. W., & Dooge, J. C. I. (1989). Attenuation and phase shift in linear flood routing. *Hydrological Sciences Journal*, *34*(1), 21–40. https://doi.org/10.1080/02626668909491306

LeFavour, G., & Alsdorf, D. (2005). Water slope and discharge in the Amazon River estimated using the shuttle radar topography mission digital elevation model. *Geophysical Research Letters*, *32*(17), L17404. https://doi.org/10.1029/2005gl023836

Lehner, B., & Grill, G. (2013). Global river hydrography and network routing: Baseline data and new approaches to study the world's large river systems. *Hydrological Processes*, *27*(15), 2171–2186. https://doi.org/10.1002/hyp.9740

Lighthill, M. J., & Whitham, G. B. (1955). On kinematic waves I. Flood movement in long rivers. *Proceedings of the Royal Society of London. Series A. Mathematical and Physical Sciences*, *229*(1178), 281–316. https://doi.org/10.1098/rspa.1955.0088

Lima, S., & Paiva, R. (2023). A simple model of flood peak attenuation: Validation dataset and example. *Mendeley Data, V1*. https://doi.org/10.17632/pjkmzh8tf8.1

McCarthy, G. T. (1938). The unit hydrograph and flood routing. In *Proceedings of Conference of North Atlantic Division* (pp. 608–609). US Army Corps of Engineers.

McMillan, H., Krueger, T., & Freer, J. (2012). Benchmarking observational uncertainties for hydrology: Rainfall, river discharge and water quality. *Hydrological Processes*, *26*(26), 4078–4111. https://doi.org/10.1002/hyp.9384

Meade, R. H., Rayol, J. M., Da Conceicão, S. C., & Natividade, J. R. (1991). Backwater effects in the Amazon River basin of Brazil. *Environmental Geology and Water Sciences*, *18*(2), 105–114. https://doi.org/10.1007/BF01704664

Merz, B., Blöschl, G., Vorogushyn, S., Dottori, F., Aerts, J. C., Bates, P., et al. (2021). Causes, impacts and patterns of disastrous river floods. *Nature Reviews Earth & Environment*, *2*(9), 592–609. https://doi.org/10.1038/s43017-021-00195-3

Meyer, A., Fleischmann, A. S., Collischonn, W., Paiva, R., & Jardim, P. (2018). Empirical assessment of flood wave celerity–discharge relationships at local and reach scales. *Hydrological Sciences Journal*, *63*(15–16), 2035–2047. https://doi.org/10.1080/02626667.2018.1557336

Mishra, A., Mukherjee, S., Merz, B., Singh, V. P., Wright, D. B., Villarini, G., et al. (2022). An overview of flood concepts, challenges, and future directions. *Journal of Hydrologic Engineering*, *27*(6), 03122001. https://doi.org/10.1061/(asce)he.1943-5584.0002164

Moody, J. A., & Troutman, B. M. (2002). Characterization of the spatial variability of channel morphology. *Earth Surface Processes and Landforms: The Journal of the British Geomorphological Research Group*, *27*(12), 1251–1266. https://doi.org/10.1002/esp.403

Moore, R. B., McKay, L. D., Rea, A. H., Bondelid, T. R., Price, C. V., Dewald, T. G., & Johnston, C. M. (2019). User's guide for the National Hydrography Dataset plus (NHDPlus) High Resolution. *Open-File Report-US Geological Survey, (2019-1096)*. https://doi.org/10.3133/ofr20191096

Moussa, R., & Bocquillon, C. (1996). Criteria for the choice of flood-routing methods in natural channels. *Journal of Hydrology*, *186*(1–4), 1–30. https://doi.org/10.1016/S0022-1694(96)03045-4

Natural Environment Research Council (NERC). (1975). Flood studies report, 1–5, London.

Paiva, R. C. D., Buarque, D. C., Collischonn, W., Bonnet, M. P., Frappart, F., Calmant, S., & Bulhões Mendes, C. A. (2013). Large-scale hydrologic and hydrodynamic modeling of the Amazon River basin. *Water Resources Research*, *49*(3), 1226–1243. https://doi.org/10.1002/wrcr.20067

Poff, N. L., Allan, J. D., Bain, M. B., Karr, J. R., Prestegaard, K. L., Richter, B. D., et al. (1997). The natural flow regime. *BioScience*, *47*(11), 769–784. https://doi.org/10.2307/1313099

Ponce, V. M. (1991a). Kinematic wave controversy. *Journal of Hydraulic Engineering*, *117*(4), 511–525. https://doi.org/10.1061/(ASCE)0733-9429(1991)117:4(511)

Ponce, V. M. (1991b). New perspective on the Vedernikov number. *Water Resources Research*, *27*(7), 1777–1779. https://doi.org/10.1029/91WR01033

Ponce, V. M. (2014). Engineering hydrology: Principles and practices (2nd ed.). Retrieved from http://ponce.sdsu.edu/enghydro/index.html

Ponce, V. M., Lohani, A. K., & Scheyhing, C. (1996). Analytical verification of Muskingum-Cunge routing. *Journal of Hydrology*, *174*(3–4), 235–241. https://doi.org/10.1016/0022-1694(95)02765-3

Ponce, V. M., & Simons, D. B. (1977). Shallow wave propagation in open channel flow. *Journal of the Hydraulics Division*, *103*(12), 1461–1476. https://doi.org/10.1061/JYCEAJ.0004892

Ponce, V. M., Taher-shamsi, A., & Shetty, A. V. (2003). Dam-breach flood wave propagation using dimensionless parameters. *Journal of Hydraulic Engineering*, *129*(10), 777–782. https://doi.org/10.1061/(ASCE)0733-9429(2003)129:10(777)

Prochaska, A. B., Santi, P. M., Higgins, J. D., & Cannon, S. H. (2008). A study of methods to estimate debris flow velocity. *Landslides*, *5*(4), 431–444. https://doi.org/10.1007/s10346-008-0137-0

Rosbjerg, D., Bloschl, G., Burn, D. H., Castellarin, A., Croke, B., Di Baldassarre, G., et al. (2013). Prediction of floods in ungauged basins: Synthesis across processes, places and scales.

Rossi, C. L. C. U., Marques, M. G., Teixeira, E. D., Melo, J. F. D., Ferla, R., & Prá, M. D. (2021). Dam-break analysis: Proposal of a simplified approach. *RBRH*, *26*. https://doi.org/10.1590/2318-0331.262120200066

Rutschmann, P., & Hager, W. H. (1996). Diffusion of floodwaves. *Journal of Hydrology*, *178*(1–4), 19–32. https://doi.org/10.1016/0022-1694(95)02824-2

Saint-Venant, A. J. C. (1871). Théorie du mouvement non-permanent des eaux avec application aux crues des rivers et a l'introduntion des Marees dans leur lit. *Comptes rendus de l'Académie des Sciences*, *73*(99), 148–154.

Sampson, C. C., Smith, A. M., Bates, P. D., Neal, J. C., Alfieri, L., & Freer, J. E. (2015). A high-resolution global flood hazard model. *Water Resources Research*, *51*(9), 7358–7381. https://doi.org/10.1002/2015WR016954

Seddon, J. A. (1900). River hydraulics. *Transactions of the American Society of Civil Engineers*, *43*(1), 179–229. https://doi.org/10.1061/TACEAT.0001414

Singh, K. P., & Snorrason, A. (1984). Sensitivity of outflow peaks and flood stages to the selection of dam breach parameters and simulation models. *Journal of Hydrology*, *68*(1–4), 295–310. https://doi.org/10.1016/0022-1694(84)90217-8

Singh, V. P., Li, J. Z., & Wang, G. T. (1998). Flood peak attenuation and forecast. *Journal of Hydrologic Engineering*, *3*(1), 20–25. https://doi.org/10.1061/(ASCE)1084-0699(1998)3:1(20)

Siqueira, V. A., Paiva, R. C., Fleischmann, A. S., Fan, F. M., Ruhoff, A. L., Pontes, P. R., et al. (2018). Toward continental hydrologic–hydrodynamic modeling in South America. *Hydrology and Earth System Sciences*, *22*(9), 4815–4842. https://doi.org/10.5194/hess-22-4815-2018

Smith, A., Sampson, C., & Bates, P. (2015). Regional flood frequency analysis at the global scale. *Water Resources Research*, *51*(1), 539–553. https://doi.org/10.1002/2014WR015814

Teng, J., Jakeman, A. J., Vaze, J., Croke, B. F., Dutta, D., & Kim, S. J. E. M. (2017). Flood inundation modelling: A review of methods, recent advances and uncertainty analysis. *Environmental Modelling & Software*, *90*, 201–216. https://doi.org/10.1016/j.envsoft.2017.01.006

Thober, S., Cuntz, M., Kelbling, M., Kumar, R., Mai, J., & Samaniego, L. (2019). The multiscale routing model mRM v1. 0: Simple river routing at resolutions from 1 to 50 km. *Geoscientific Model Development*, *12*(6), 2501–2521. https://doi.org/10.5194/gmd-12-2501-2019

Tsai, C. W., & Yen, B. C. (2001). Linear analysis of shallow water wave propagation in open channels. *Journal of Engineering Mechanics*, *127*(5), 459–472. https://doi.org/10.1061/(ASCE)0733-9399(2001)127:5(459)

U.S. Army Corps of Engineers (USACE). (2020). *HEC-RAS River Analysis System: Hydraulic Reference Manual, Version 6.0*. Hydrologic Engineering Center. Retrieved from www.hec.usace.army.mil

U. S. Bureau of Reclamation. (1989). *Policy and procedures for dam safety modification decision making* (p. 302). Department of Interior.

Wahl, T. L. (1998). *Prediction of embankment dam breach parameters: A literature review and needs assessment*. Dam Safety Report U.S. Department of the Interior, Bureau of Reclamation.

Wetmore, J. N., & Fread, D. L. (1981). *The NWS simplified dam-break flood forecasting model* (pp. 164–197). National Weather Service.

Wong, T. H., & Laurenson, E. M. (1983). Wave speed–discharge relations in natural channels. *Water Resources Research*, *19*(3), 701–706. https://doi.org/10.1029/WR019i003p00701

Wong, T. S., & Zhou, M. C. (2006). Kinematic wave parameters for trapezoidal and rectangular channels. *Journal of Hydrologic Engineering*, *11*(2), 173–183. https://doi.org/10.1061/(ASCE)1084-0699(2006)11:2(173)

Wood, E. F., Roundy, J. K., Troy, T. J., Van Beek, L. P. H., Bierkens, M. F., Blyth, E., et al. (2011). Hyperresolution global land surface modeling: Meeting a grand challenge for monitoring Earth's terrestrial water. *Water Resources Research*, *47*(5), W05301. https://doi.org/10.1029/2010WR010090

Yamazaki, D., Kanae, S., Kim, H., & Oki, T. (2011). A physically based description of floodplain inundation dynamics in a global river routing model. *Water Resources Research*, *47*(4), W04501. https://doi.org/10.1029/2010WR009726

Yevjevich, V. M. (1964). *Bibliography and discussion of flood-routing methods and unsteady flow in channels (No. 1690-1695)*. US Government Printing Office.